Tonal Noise Control Versus Performances on NACA0015 Hydrofoil

Paul Francois, Basile Lère, Xavier Amandolese, Jacques-André Astolfi

Tonal Noise Control Versus Performances on NACA0015 Hydrofoil

Paul Francois
IRENav French Naval Academy, France, paul.francois@ecole-navale.fr.

Basile Lère
IRENav French Naval Academy, France.

Xavier Amandolese
LMSSC Cnam, France.

Jacques-André Astolfi
IRENav French Naval Academy, France.

Manuscript received June 02, 2023; accepted as submitted June 17, 2023.

Abstract. Strong correlation between boundary layer excitation and hydrofoil eigenmode occur for specific angles of attack and Reynolds numbers, resulting in strong tonal noise emissions under certain circumstances. This study aims to analyze the performance of vibration control methods such as truncated trailing edge or boundary layer triggering. The study explores the conditions for hydroelastic trailing edge vibrations on a hydrofoil clamped in a hydrodynamic tunnel, with tests performed for Reynolds numbers up to 1.2×10^6 and various angles of attack up to 10°. Experiments were conducted on a clamped 0.1 m chord NACA0015 aluminum hydrofoil, with measurements taken for both vibrations and hydrodynamic components such as lift, drag, and moment. The goal of the study is to closely understand the impact of vibration control on hydrofoil efficiency. This could be very beneficial for those who are working on optimizing profile design. The study first presents the experimental setup, followed by an analysis of the hydrofoil's vibratory response and a presentation of the effectiveness of control solutions. Then, the performance of these solutions are discussed followed by a conclusion.

Keywords: Fluid-structure interaction; Trailing edge vibration; Transition induced vibrations; Tonal noise; Tollmien Schlichting waves

NOMENCLATURE

c	Hydrofoil chord length [m]
C_d	Drag coefficient [-]
C_l	Lift coefficient [-]
C_m	Moment coefficient [-]
f	Frequency [Hz]
U_∞	Flow velocity [m s^{-1}]
x	Position on the hydrofoil chord [m]
Re	Reynolds number [-]
St	Strouhal number [-]

α	Angle of attack [deg.]
δ	Boundary layer thickness [m]
ν	Kinematic viscosity [m^2 s^{-1}]

DMD	Dynamic Mode Decomposition
DNS	Direct Numerical Simulation
LSB	Laminar Separation Bubble
TR-PIV	Time Resolved Particle Image Velocimetry
TS	Tollmien-Schlichting

1 INTRODUCTION

Noise and vibrations of hydrodynamic lifting surfaces are a matter of great concern since they can affect performances, cause structural failures, disturb users, impact acoustic discretion and the entire ecosystem. According to Blake (1984), three unsteady flow mechanisms can be responsible for the vibration of a hydrofoil operating at a low angle of attack. The first one is due to the unsteadiness of the incoming flow, which generates unsteady random hydrodynamic loading and a so-called buffeting response of the hydrofoil. The second one can also be referred as turbulence-induced vibration but in that case, it is due to the boundary layer on the hydrofoil surface. It thus mainly concerns hydrofoils operating at high Reynolds numbers. The third one is due to a tonal flow excitation generated by periodic vortex shedding from the trailing edge.

For hydrofoils with a blunt trailing edge, the vortex wake organization can be regarded as a Kármán vortex street, as for the canonical circular cylinder configuration. But for hydrofoils with a sharp trailing edge, the exact mechanism responsible for the discrete frequency organization of the wake remains unclear. In that context, the work done on airfoil tonal noise in the last decades is of great interest.

The first mention of discrete frequency tones from a sharp-trailing-edge airfoil at moderate Reynolds number is probably due to Clark (1971). Paterson et al. (1973) also mentioned tonal noise on airfoil at Reynolds numbers close to 8×10^5 at a small angle of attack of $\alpha = 6°$.

Tam (1974) questioned the simple Strouhal number correlation and the Kármán vortex-type organization of the wake and proposed that the tones are generated by a self-excited feedback loop involving unstable disturbances in the boundary layer and in the wake flow, along with the feedback of acoustic waves. Using this feedback loop model, a ladder-type evolution of the dominant frequency based on Shen (1954) and Lin (1944) stability curves can be drawn. Following the work of Paterson et al. (1973) and Tam (1974), Arbey and Bataille (1983) assumed that the ladder-type evolution of the frequency can be due to an aeroacoustic feedback loop involving the diffraction of Tollmien-Schlichting (TS) instabilities by the trailing edge and the maximum velocity point of the airfoil. In an attempt to clarify the mechanism of tonal noise generation on aerofoils at moderate Reynolds numbers, Nash et al. (1999) conducted experiments on a NACA0012 aerofoil section at an incidence angle of 6°. They showed that the ladder-type evolution of tones could be eliminated under anechoic conditions. Their results also revealed the presence of strongly amplified boundary-layer instabilities just upstream of the pressure surface trailing edge, which roll up to form a regular Kármán-type vortex street. They proposed a new mechanism for tonal noise generation based on the growth of T-S instability waves amplified by inflectional profiles in the separating laminar shear layer on the pressure surface. They also demonstrated, thanks to flow visualisation, that the flow at the trailing edge is organized as a coherent structure.

In another paper, McAlpine et al. (1999) concentrated their work on the stability of the pressure-side boundary layer to understand the relationship between T-S waves and tonal noise. They conducted experiments on two airfoils, including an asymmetrical one, which allowed them to show the impact of

airfoil shape on the tonal noise frequency. They also confirmed that tonal noise is closely dependent on the presence of a Laminar Separation Bubble (LSB) on the pressure side close to the trailing edge.

Nakano et al. (2007) carried out experiments that allowed them to clarify the impact of the angle of attack on the tonal noise mechanism at a moderate Reynolds number of $Re = 1.6 \times 10^5$. Using liquid-crystal visualization and particle image velocimetry, they confirmed that an LSB moves along the foil on both the suction and pressure sides as a function of the angle of attack. They also showed that tonal noise apparition is strongly linked to the location of the reattachment point of the LSB near the trailing edge on the pressure side at low angles of attack.

More recently, Pröbsting and Yarusevych (2015) investigated a NACA0012 airfoil emitting tonal noise. They found that for an angle of attack of 1.2° and for $Re \leq 4.5 \times 10^5$, tonal noise emission could also be due to an acoustic feedback involving an LSB formed on the suction side of the airfoil. These different studies did not take into account hydrofoil vibrations. Conversely, Ducoin et al. (2012) observed a discrete frequency excitation mechanism involving an LSB on the suction side of a hydrofoil thanks to vibratory response. Based on experiments conducted on a NACA66312 laminar hydrofoil at low angles of attack and transitional Reynolds numbers, they showed that the frequency of the boundary-layer transition mechanism can couple with some natural frequencies of the hydrofoil leading to significant vibrations.

Ducoin and Astolfi (2019) described a vortex shedding of the LSB using a NACA66 hydrofoil instrumented with pressure sensors at $4°$. Pressure fluctuations at the transition region showed strong coherent, periodic, and intermittent behavior when downstream fluctuations showed more random fluctuations with smaller amplitudes, which clearly demonstrate turbulent flow.

They also showed a strong frequency correlation between measurement and Direct Navier-Stokes (DNS) simulations. They found a linear increase of the LSB vortex shedding frequency with Reynolds numbers. DNS calculations shows consistent structure associated with the development of TS waves and a quick disappearance of LSB vortex shedding periodicity from $x/c = 0.7$ to $x/c = 0.85$.

Following the study of Francois et al. (2022), the objective of the current research is to investigate the effects of different control methods of strong hydroelastic coupling on the performance of a symmetric NACA0015 hydrofoil operating at moderate Reynolds numbers. The experimental setup and the hydrofoil's modal characteristics are presented in Section 2. Section 3 reports the results and discussions, which mainly focus on drag, lift-drag ratio, and moment, followed by a conclusion.

2 MATERIALS AND METHODS

Experiments were performed in the hydrodynamic tunnel of the French Naval Academy Research Institute (IRENav) in a square test section of 0.19 m $\times$ 0.192 m with a honeycomb standardized inlet flow (Fig. 1). An aluminum NACA0015 section hydrofoil with a Young's modulus of 69 GPa, a constant chord of 0.1 m, a span of 0.191 m, and a confinement parameter $h/c = 1.92$ was mounted in a three-component force measurement system. The flow speed was regulated up to 12 m s^{-1}, corresponding to a Reynolds number range referred to the chord up to 1.2 $\times$ 10^6.

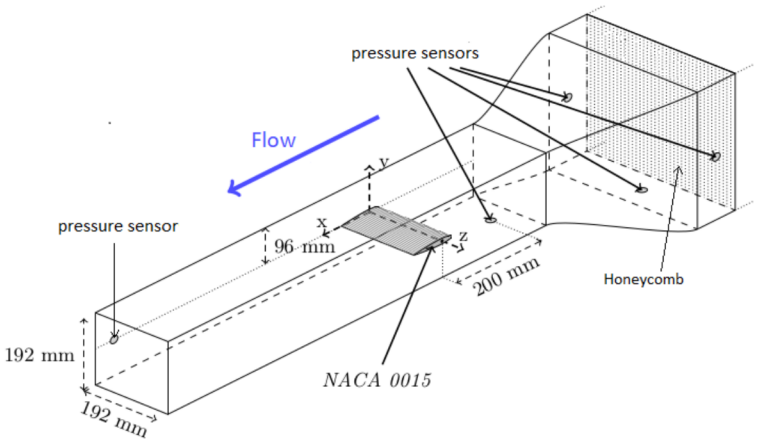

Figure 1. Clamped-free hydrofoil model in the IRENav hydrodynamics test section.

2.1 Vibrations and Eigenmodes

Vibrations measurements were performed in an hydrofoil clamped along the chord in one side and free in the other (Fig. 2). They were carried out at a point located at 70% from the leading edge and 64% of the span using a PSV-400 vibrometer that operates based on the Doppler-effect, with a minimum precision of 0.02 μm s^{-1}. To limit the impact of pump vibrations, the sensor was separated from the tunnel structure. A 3M®S80 patch film was applied to the suction side of the profile to improve the signal quality. To ensure reliable results and avoid spectral overlap, all vibrations spectra were calculated using fast Fourier transform on an average of 16 data samples collected for 1 second at a frequency acquisition rate of 9.6 kHz.

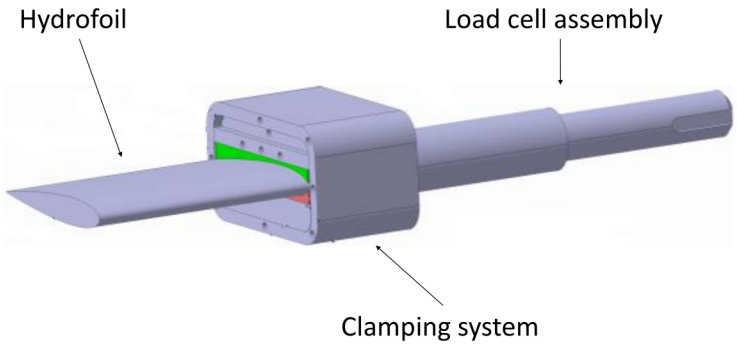

Figure 2. Schematization of the hydrofoil mounting.

The 830 Hz eigenmode exhibits the highest amplitude of vibration in the Reynolds number range studied. This mode shows a high deformation area close to the trailing edge, with a maximum at mid-span, consistent with the trailing edge phenomena observed in previous studies (Nash et al., 1999). This eigenmode is labeled ”mode 4” and is referred to the flapping trailing edge mode.

2.2 Particle Image Velocimetry Analysis

Time-Resolved Particle Image Velocimetry (TR-PIV) was performed using a SpeedSense 2640 Phantom camera, capturing frames of 1024 pixels x 400 pixels at 10 kHz and with a Nd-Yag double cavity laser. Post-processing was carried out using DynamicStudio® software from Polytech®, with an inter-

rogation area of 8 pixels x 8 pixels and a 4 pixels recovery. This resulted in a 251 pixels x 98 pixels vector fields with an uncertainty of 11% compare to the mean flow velocity (Charonko and Vlachos, 2013) . For each acquisition, 2000 images were collected over a duration of 0.2 seconds.

Dynamic Mode Decomposition (DMD) was performed using the Wrapper algorithm developed by Zigunov (2022) to identify wake coherent structures. Schmid (2010) demonstrated that the DMD method allows extraction of dynamic information from experimental flow and can be used to describe physical mechanisms. The DMD reconstruction presented in this article consists of spatial TR-PIV flow speed vectors associated with the frequency exhibiting the highest spatial consistency.

2.3 Lift and Drag

Measurement campaigns were performed with the hydrofoil profile mounted on a clamped structure to increase the accuracy of the vibration measurements. The entire system was assembled on a two-axis hydrodynamics balance which measured instantaneous lift, drag and moment.

To ensure reliability, measurements were performed twice, each time with increasing and decreasing angles of incidence. Moment measurement was performed at the center of rotation of the hydrofoil which is 25% of the chord. Dimensionless pressure center location was also deduced as $1/4 - C_m/C_l$ where C_m is the pitching moment coefficient about the quarter chord point and C_m the lift coefficient.

Measurement error is a crucial aspect to ensure reliable comparison of performance results. The maximum error was found to be less than 2% of the measuring system margin for all three components. Therefore, this 2% value was taken into account as the error for the entire study. For readability, the error was not included in the figures, as it was deemed small enough to be neglected for comparisons.

2.4 Control Method

Two methods have been implemented to control vibrations and tonal noise emission.

The first one, called tripped, involved artificially triggering turbulence at the pressure side using a roughness strip of 4 $\times$ 10^{-6} m height, 0.01 m width, and 175 $\times$ 10^{-6} m thickness. As mentioned by Paterson et al. (1973), a roughness strip can be used to control boundary layer development and suppress tonal noise emission. This strip was positioned at 50% chord of the pressure side of the hydrofoil.

The second method, called 'truncated', is commonly used in the industry and involves truncating the hydrofoil's trailing edge. This was performed on a hydrofoil with the same material and geometry as the free configuration. The truncation was made at 95% of the chord, generating a trailing edge thickness of 0.002 m. Coefficients such as lift and drag were calculated using a chord length of 0.1 m to ensure proper comparison of results.

3 RESULTS AND DISCUSSIONS

3.1 Vibrations

The measured vibratory responses of the hydrofoil at different root angles of attack for a fixed Reynolds number of 8×10^5 are shown in Fig. 3. The results indicate that trailing edge vibrations occur within a specific range of angle of attack ($4° \leq \alpha \leq 8°$) and that modes 1, 2, and 3 are present with broadband excitation across the entire incidence range, respectively at 50, 200, and 290 Hz. Eigenmode 4 coupling appears to be sensitive to the angle of attack at this specific Reynolds number, with a slight frequency shift observed. In particular, the coupling frequency shows a slight decrease within the angle of attack range between 6° and 8°.

Fig. 4 shows the maximum amplitude of vibratory response for the three studied cases as a function

of the Reynolds number, at an angle of attack of 5°. The truncated case shows a coupling succession of the different eigenmodes of the hydrofoil. The main difference with the free configuration is the coupling Reynolds number for mode 4, which is significantly higher (7.2×10^5 instead of 6.1×10^5). The opposite phenomenon can be observed for mode 2, where coupling in the truncated case remains active for a higher flow speed. This is not the case with mode 4, where the decoupling Reynolds number is the same. The amplitudes of the response are slightly higher for the truncated case. Therefore, the truncated method represents an advantage in reducing the coupling range for mode 4, which is responsible for tonal noise emission. However, it has the disadvantage of increasing the coupling range of mode 2 and slightly amplifying the vibration amplitudes.

For the tripped case, the amplitude remains significantly lower, except for very low Reynolds numbers below 2.3×10^5. The vibration level is similar to the two other cases one, without coupling. The frequencies indicate that only eigenmodes 1 and 2 couple with the flow field, and mode 4 remains inactive. Therefore, the tripped method appears to be a very effective solution to eliminate vibration and tonal noise caused by the coupling of eigenmode 4.

3.2 Wake Analysis

In free configuration a coherent structure in space and frequency has been highlighted in the wake using TR-PIV and Dynamics Mode Decomposition when strong mode 4 coupling occurs (as shown in Fig. 5, hydrofoil trailing edge in the top left corner). This structure appears as a vortex street at the same frequency as the vibratory response, and grows until 120% of the chord before decreasing in intensity. Such structures, known as Kármán street, can be an important source of drag.

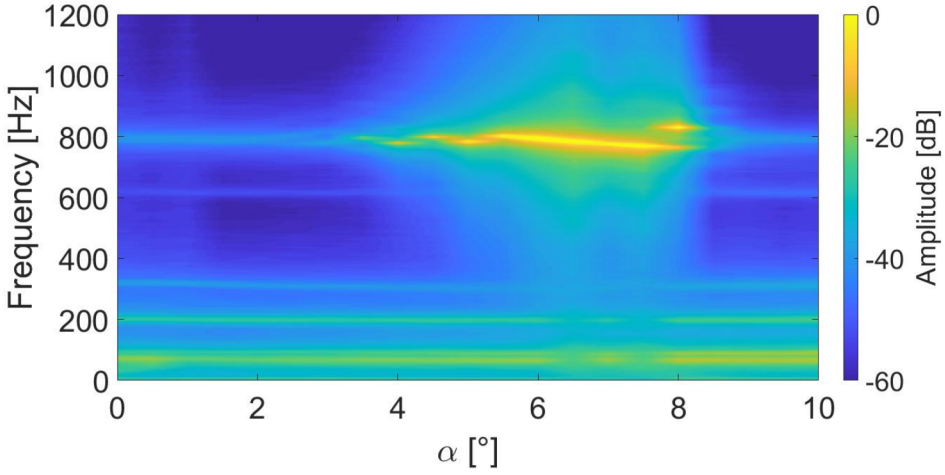

Figure 3. Vibratory response of free hydrofoil as a function of angle of attack for $Re = 8 \times 10^5$.

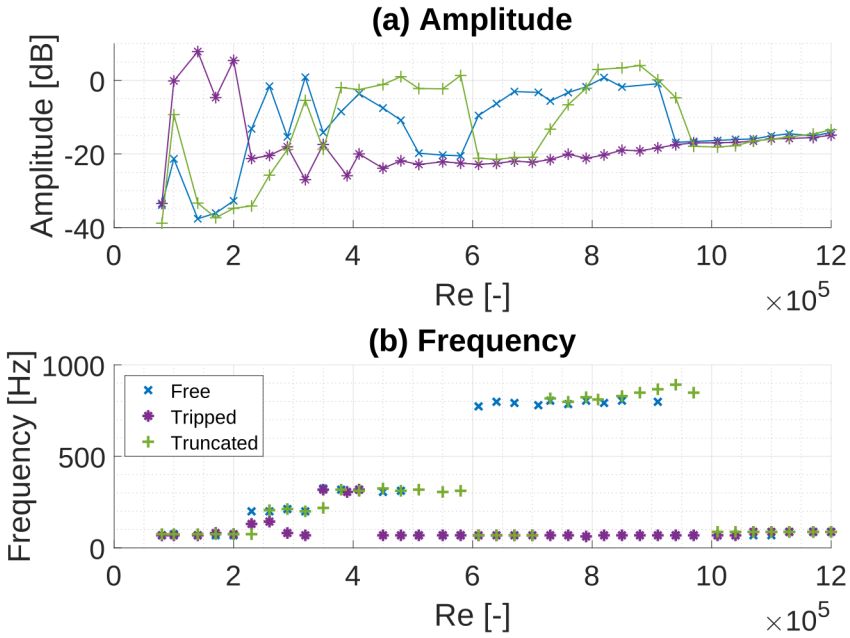

Figure 4. Amplitude and frequency of dominant vibrational peak for free, tripped and truncated cases as a function of Reynolds number at α =5°.

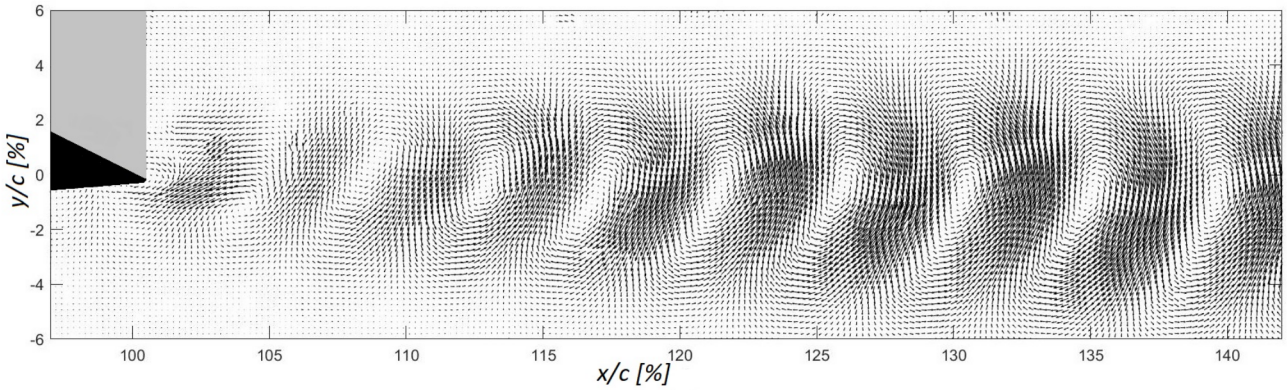

Figure 5. DMD mode shape of the wake for free configuration at frequency of 783 Hz for $Re = 8 \times 10^5$ and α =5°.

No discernible structure has been detected out of the coupling angles or in tripped configuration. This suggests that they are a product of hydrofoil coupling, and the control methods used may have an effect on the hydrodynamic coefficients.

3.3 Drag

The drag coefficient for all cases is presented in Fig. 6 as a function of incidence for a Reynolds number of 8×10^5. It can be observed that the drag is significantly higher for the truncated method than for the free configuration, and this is the case for all angles, although the curve shapes are similar. A slight bump in drag can be noticed between 5.5° and 7.5° for the truncated method compared to the free configuration, even though the curve shapes are similar. The same phenomenon appears in the free case beyond 6°, which corresponds to the beginning of strong trailing edge coupling. This change is so significant that it reaches tripped drag between 7° and 7.5° and remains higher until it decreases after 8°.

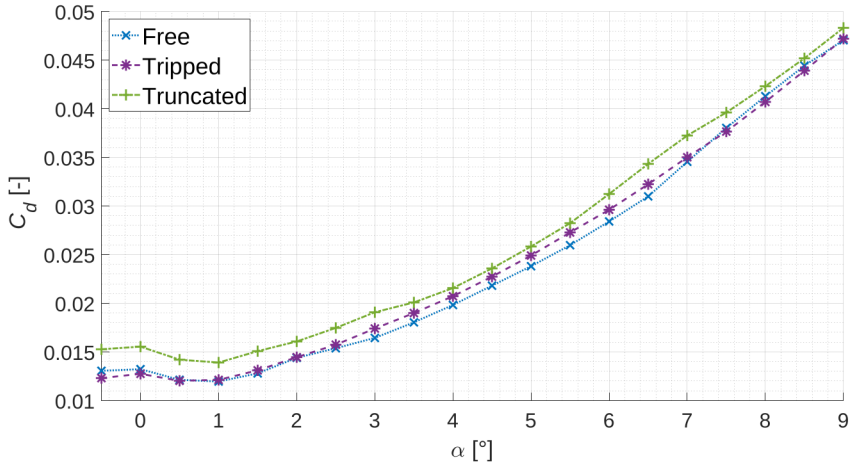

Figure 6. Variation of drag coefficient with angle of attack for three cases at $Re = 8 \times 10^5$.

This angle of 8° corresponds to the maximum angle where coupling occurs. Therefore, it is possible that this bump in the drag for free and truncated configurations corresponds to the coupling effect. In contrast, the tripped curves appear without any significant phenomena except for very low angles lower than 1° where it seems to have the least drag among the three methods.

3.4 Lift-drag Ratio

Performance of these two control methods has been studied. The lift-drag ratio is presented in Fig. 7 as a function of the angle of attack for a Reynolds number of 8×10^5. The right axis presents the loss of performance relative to the free configuration. Truncated configuration appears to have a significant impact on performance. Close to the maximum performance (around 6°), the loss is about 10%.

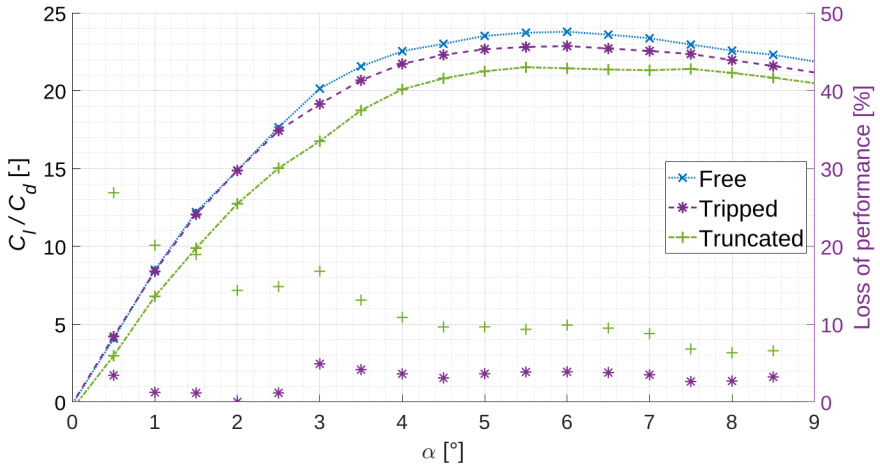

Figure 7. Variation of lift-drag ratio with angle of attack for free, tripped and truncated configuration at $Re = 8 \times 10^5$.

For the tripped method, the difference in performance is much lower with less than 4% performance loss at the maximum lift-drag ratio angle. Moreover, this loss is much less pronounced for angles smaller than 3.5°. For both cases, the tendency is a decreasing performance loss with the angle of

attack.

3.5 Moment

As explained in section 2.3, the moment can be analyzed by examining the position of the pressure center location using the lift value. Moment coefficient and pressure center location are presented in Fig. 8.

For the free configuration, a strong increase in the moment coefficient can be observed from 5.5° which corresponds to the appearance angle of strong coupling with tonal noise emission. After 8°, where the coupling disappears, the moment coefficient decreases suddenly. As a consequence the pressure center location is shifted toward the leading-edge when the coupling occurs.

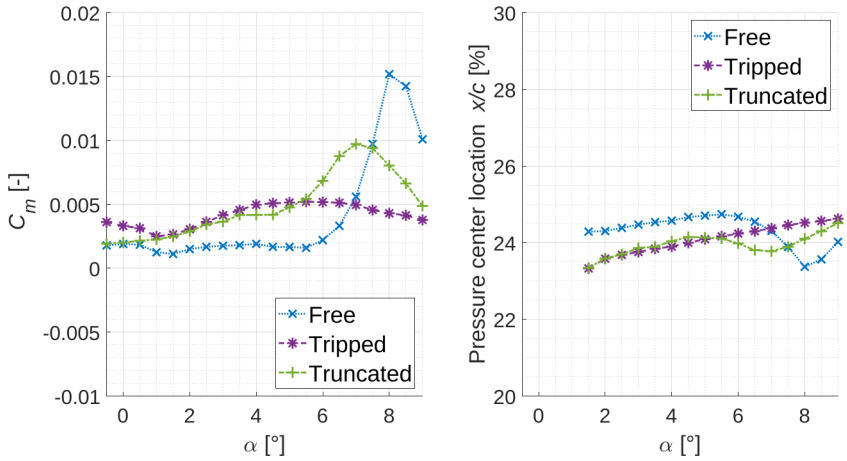

Figure 8. Moment coefficient and pressure center location with angle of attack for free, tripped and truncated configuration at $Re = 8 \times 10^5$.

Conversely, for the tripped configuration where no coupling occurs, there is no bump in the moment coefficient, which shows that bump is linked to trailing edge eigenmode coupling. The pressure center location linearly goes toward the trailing edge with the angle of attack increasing.

Truncated configuration shows the same behavior as free one except that the pressure center location shift appears between 4°and 7°. This can be explained by the chord reduction of the hydrofoil. The proximity of boundary layer transition to the trailing edge is a key point for trailing edge eigenmode coupling. The transition point is also known to move rearward the trailing edge with angle of attack on the pressure side. Thus, a reduction of the chord length could lead to a shift of the coupling angles.

3.6 Discussion

A previous work has demonstrated that the state of the boundary layer at the trailing edge is a key parameter for strong coupling with the trailing edge eigenmode and tonal noise emission.

Dynamic Mode Decomposition reveals a well-organized vortex shedding structure during trailing edge eigenmode coupling. This phenomenon is generated by the vibrations of the profile under excitation, which explain the good agreement between the trailing edge vortex shedding frequency and hydrofoil vibrations. This could also be considered as a source of significant drag.

The tripped configuration shows no identified pattern on the wake, as vibratory responses confirm the efficiency of triggered boundary layer on the trailing edge coupling and tonal noise emission. However,

vortex shedding deletion is not sufficient to compensate the loss in lift-drag ratio, although its effect can be seen in drag. The truncation configuration, however, is shown to be an important source of drag, which has a strong impact on the lift-drag ratio. Although it has a smaller angle coupling range than the free hydrofoil, the amplitudes of coupling can be higher. Nevertheless, the advantage of this configuration on vibration and tonal noise emission is less impressive than the triggered boundary layer one. In terms of performance, it seems that truncation has a strong negative impact, twice more important than the tripped configuration.

Results show that the coupling phenomenon also has an impact on the moment coefficient, with a setback of the hydrodynamic pressure center location for both the free and truncated configurations, in contrast to the tripped configuration. The shift in incidences observed for truncated configuration can be explained by the chord reduction of the hydrofoil. This setback can be considered as a signature of coupling, which is completely eliminated by triggered pressure-side boundary layers.

4 CONCLUSIONS

The experimental analysis of tonal noise control methods has shown that triggering the pressure side boundary layer is an effective approach that completely eliminates the vibration coupling responsible for acoustic waves. The commonly used truncated trailing edge method also showed an impact on vibratory response, but to a much smaller extent. In addition to their impact on vibration, lift and drag results revealed a loss of performance with these control methods, although energetic vortex shedding was observed at the coupling. The loss of performance was more significant for the truncated method than the triggered one. Moment coefficient analysis also revealed a strong impact of coupling on it. The triggered configuration has been shown to be a powerful method to suppress tonal noise emission, which is challenging for the environment, by eliminating the strong vibrations that can cause structural failures. It also suppresses moment events that can be problematic for stability much better than truncating the hydrofoil in terms of performance.

REFERENCES

Arbey, H. and J. Bataille (1983). Noise Generated by Airfoil Profiles Placed in a Uniform Laminar Flow. In: *Journal of Fluid Mechanics* 134, pp. 33–47.

Blake, W. K. (1984). Excitation of Plates and Hydrofoils by Trailing Edge Flows. In: *Journal of Vibration and Acoustics* 106, pp. 351–363.

Charonko, J. and P. Vlachos (2013). Estimation of Uncertainty Bounds for Individual Particle Image Velocimetry Measurements from Cross-Correlation Peak Ratio. In: *Measurement Science and Technology* 24.6, p. 065301.

Clark, L. T. (1971). The Radiation of Sound from an Airfoil Immersed in a Laminar Flow. In: *J. Eng. Gas Turbines Power* 93.4, pp. 366–376.

Ducoin, A. and J. A. Astolfi (2019). Wall-Pressure Fluctuations of Laminar Separation Bubble Based on Direct Numerical Simulation and Experiments Over a Hydrofoil at Re= 450,000. In: *European Journal of Mechanics-B/Fluids* 76, pp. 132–144.

Ducoin, A., J. A. Astolfi, and M. L. Gobert (2012). An Experimental Study of Boundary-Layer Transition Induced Vibrations on a Hydrofoil. In: *Journal of Fluids and Structures* 32, pp. 37–51.

Francois, P., J. A. Astolfi, and X. Amandolese (2022). Experimental Analysis of Hydrofoil Hydroelastic Trailing Edge Vibrations. In: *Actes du 25ème Congrès Français de Mécanique*. Nantes: CFM 2022.

Lin, C. C. (1944). On The Stability of Two-Dimensional Parallel Flows. In: *Proceedings of the National Academy of Sciences* 30.10, pp. 316–324.

McAlpine, A., E. C. Nash, and M. V. Lowson (1999). On the Generation of Discrete Frequency Tones by the Flow Around an Aerofoil. In: *Journal of Sound and Vibration* 222.5, pp. 753–779.

Nakano, T. et al. (2007). Experimental Study on Flow and Noise Characteristics of NACA0018 Airfoil. In: *Journal of Wind Engineering and Industrial Aerodynamics* 95.7, pp. 511–531.

Nash, E. C., M. V. Lowson, and A. McAlpine (1999). Boundary-Layer Instability Noise on Aerofoils. In: *Journal of Fluid Mechanics* 382, pp. 27–61.

Paterson, R. W. et al. (1973). Vortex Noise of Isolated Airfoils. In: *Journal of Aircraft* 10.5, pp. 296–302.

Pröbsting, S. and S. Yarusevych (2015). Laminar Separation Bubble Development on an Airfoil eEitting Tonal Noise. In: *Journal of Fluid Mechanics* 780, pp. 167–191.

Schmid, P. J. (2010). Dynamic Mode Decomposition of Numerical and Experimental Data. In: *Journal of fluid mechanics* 656, pp. 5–28.

Shen, S. F. (1954). Calculated Amplified Oscillations in the Plane Poiseuille and Blasius Flows. In: *Journal of the aeronautical sciences* 21.1, pp. 62–64.

Tam, C. K. W. (1974). Discrete Tones of Isolated Airfoils. In: *The Journal of the Acoustical Society of America* 55.6, pp. 1173–1177.

Zigunov, F. (2022). *Dynamic Mode Decomposition [DMD] - Wrapper.*